Tribology Letters (2022) 70:2
https://doi.org/10.1007/s11249-021-01540-9

ORIGINAL PAPER

Increased Sliding Friction of a Lubricated Soft Solid Using an Embedded Structure

Nichole Moyle[1] · Hao Dong[1] · Haibin Wu[2] · Constantine Y. Khripin[3] · Chung-Yuen Hui[2] · Anand Jagota[1,4]

Received: 25 July 2021 / Accepted: 2 November 2021

Abstract

Controlling the lubricated sliding friction of compliant contacts is important for many mechanical and biological systems. Multiphase materials have been shown to exhibit varied lubricated friction responses when compared to controls of just one phase of the material. In this work, we describe a structured two-phase material composed of a plastic mesh embedded in a compliant elastomer matrix. This embedded mesh structure (EMS) exhibits increased lubricated sliding friction for a number of load, velocity, and lubricant viscosity conditions. The observed friction enhancement appears to be a result of the EMS sample transitioning to the mixed lubrication regime under conditions in which the control is in the elastohydrodynamic lubrication regime. Simulations suggest that the difference in lubrication regimes for the EMS sample compared to the unstructured control comes from areas of high contact pressure induced by the increased local contact stiffness of the material near the embedded mesh. We hypothesize that these areas of high pressure can lead to the destabilization of lubricant films under conditions where the control films are stable, leading to the difference in lubrication regime behaviors observed.

Graphical Abstract

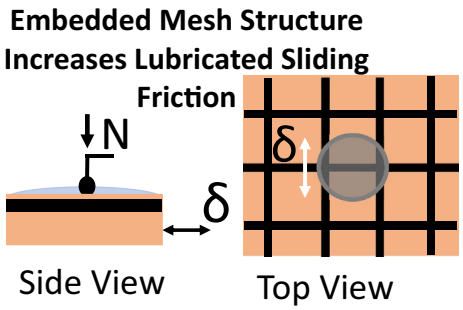

Keywords Lubrication · Friction · Enhancement · Elastohyrodynamic lubrication

1 Introduction and Background

The ability to alter and control lubricated sliding behavior in compliant materials can benefit a number of mechanical and biological systems. Mechanical systems include anti-slip safety shoes [1, 2], tires sliding on a wet road [3–8], and elastomeric seals [9] while biological systems include contact lenses [10, 11] and wet skin contact applications [12, 13]. Recently a two-phase periodic structure (TPPS) was developed using two elastomers with varied modulus to obtain enhancement (where by enhancement we mean

✉ Anand Jagota
anj6@lehigh.edu; nma315@lehigh.edu

1 Department of Chemical and Biomolecular Engineering, Lehigh University, Bethlehem, PA, USA

2 Department of Mechanical and Aerospace Engineering, Cornell University, Ithaca, NY, USA

3 Michelin North America Inc., Greenville, SC, USA

4 Department of Bioengineering, Lehigh University, Bethlehem, PA, USA

Published online: 19 November 2021

increase) in the lubricated sliding friction of the system [14]. This structure produced enhancements in the elastohydrodynamic lubrication (EHL) regime through an additional mechanism for dissipation of energy as the system alternated between sliding on regions of two different compliances. There are several ways in which a structure could be developed to produce a spatially varying contact compliance, raising the question if similar behavior would be observed for such alternate structures. In this work, an embedded mesh structure (EMS) was developed which also produced enhancements in the lubricated sliding friction of the system; however, the mechanism of enhancement appears to be different.

The lubricated sliding behavior of elastic contacts has been extensively studied [15–17] often for stiff surfaces such as the metal contacts that occur in machinery [18–21]. Stiff elastic contacts can be modeled accurately using the Reynolds lubrication theory [15–17]. For highly compliant materials, additional effects to those which are captured by standard Reynolds lubrication theory must be considered, such as the changes in pressure and liquid-film thickness profiles due to material deformations as well as hysteretic forces [17, 22–26]. A number of geometries have been experimentally investigated for the lubricated sliding behavior of compliant contacts such as sphere-on-flat [27–33], ring-on-disk [34], and roll-on-disk [35] geometries. These studies have investigated the effects of properties such as surface roughness, lubricant viscosity, viscoelasticity, and material modulus. The effect of these properties on the lubricated sliding behavior of the system is heavily dependent on the lubrication regime in which the system is operating.

Typically, at low loads and high velocities and viscosities, a system operates in the hydrodynamic lubrication regime [15] where there is a continuous layer of fluid between the two contacting surfaces at all times. When pressures are large enough that one or both of the contacting surfaces experiences significant deformation, but there is still a full fluid film present, the system is defined to be in the elastohydrodynamic lubrication (EHL) regime [16]. Compliant material systems are typically in the EHL regime when a full fluid film is present, as they deform at fairly low pressures. As load is increased and the velocity and/or viscosity are decreased, a system will next enter the mixed lubrication regime [22]. Here, there is still a fluid film present between the opposing solid surfaces in much of the effective contact region, but areas of solid–solid contact are also present. Due to the areas in solid–solid contact, in this regime, adhesive and viscoelastic forces often contribute significantly to the overall friction response of the materials. Finally, at high loads and low velocities and viscosities, the system will typically enter the boundary lubrication regime. Here the fluid film has been mostly expelled and is no longer playing a role in the mechanics of the system; thus, the system behaves similarly to a dry contact [22, 23].

Depending on the lubrication regime a system is in, different methods can be used to adjust the friction properties. One of these methods involves designing multiphase materials as one of the contacts, as seen with the particle-filled tire system. It has been shown that carbon black particles and silica particles produce different lubricated sliding responses when added to rubber composites [6–8, 36, 37]. Surface texturing has been utilized to decrease friction between lubricated rigid contacts [38]. In compliant materials, surface texturing has been used to increase sliding friction under lubricated conditions [39–41].

In dry friction, not only surface texturing is widely used to control the friction and adhesion properties of compliant elastomers, but also flat surfaces with internal structure have been shown capable of such enhancements [42–48]. For lubricated conditions, the previously mentioned TPPS, which had a flat surface but a periodic structure based on its varying modulus, exhibited an increase in lubricated sliding friction when the system was in the EHL regime [14]. This structure utilized the periodic variation of elastic and potential energy during sliding to increase friction. The demonstration of the TPPS in obtaining lubricated sliding friction enhancement via a flat yet structured elastomer suggests alternate designs to create a periodically varying local contact modulus could also provide friction enhancements. One such design is described in this work, where we have developed an EMS as a two-phase material that combines a compliant elastomer bulk with a stiffer plastic mesh structure embedded under the contacting surface. This structure produces significant lubricated sliding friction enhancements when compared to a control but by a different mechanism than the TPPS structure.

2 Materials and Methods

2.1 Sample Fabrication

EMS samples were fabricated by encasing one layer of plastic mesh (UV-Resistant Plastic Mesh, McMaster-Carr Catalog No. 87655K11) in a silicone elastomer (poly(dimethylsiloxane), Dow Sylgard 184, Dow Corning) matrix. The plastic mesh had a mesh opening size of 1.59 mm and a wire diameter of 0.41 mm with a period of 2 mm. During fabrication, the mesh was suspended 0.15 mm above the bottom of a petri dish using spacers, and a 2 mm thick sample of PDMS with a 30:1 base to crosslinker weight ratio was cast around the mesh. The assembly was cured at 80 °C for 2 h. Figure 1a shows an image of the final EMS sample, and Fig. 1b shows a schematic detailing the key dimensions of the EMS sample. The Young's modulus

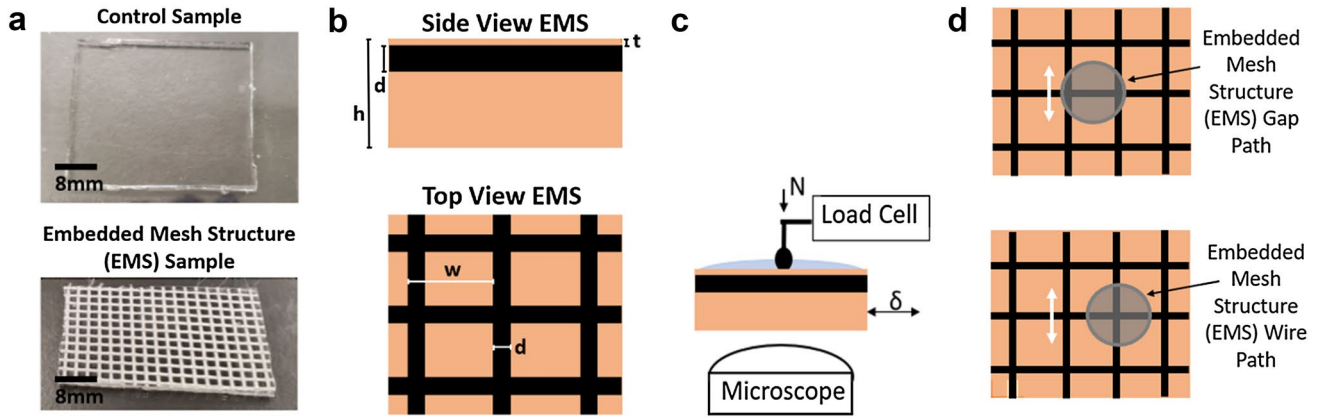

Fig. 1 **a** Image of control sample (top) and embedded mesh structure (EMS) sample (bottom). **b** Schematic of EMS sample showing relevant dimensions where $h=2$ mm, $d=0.41$ mm, $t=0.15$ mm, and $w=2$ mm. **c** Schematic of lubricated sliding experimental setup on an EMS sample. Orange color indicates 30:1 PDMS matrix while the black line indicates side view of embedded mesh. **d** Schematics showing two different sliding paths on the embedded mesh structure. In the top schematic, the gap path is shown, in which the center of the indenter periodically passes over the center of the gap in the mesh. In the bottom schematic, the wire path is shown, in which the center of the indenter travels over the continuous wire portion of the mesh (Color figure online)

of the PDMS used was approximately 120 kPa (See SI, S.6 for measurement details). The EMS structure was compared to a homogenous unstructured control sample fabricated by casting a 2 mm slab of 30:1 base to crosslinker ratio PDMS and curing at 80 °C for 2 h. An image of the control sample can be found in Fig. 1a.

2.2 Lubricated Friction Experiments

Figure 1c shows a schematic of the experimental setup for the lubricated sliding experiments. EMS samples were tested on the surface under which the mesh was embedded at a depth of approximately 0.15 mm. Silicone oil of three different viscosities was used as a lubricant ($\eta=0.97$, 9.7, and 97 Pa*s; Sigma Aldrich Silicone Oil #s 378399, 378402, and 378437). A spherical glass indenter ($R=2$ mm) was used as the other contacting surface and was brought vertically into contact with the samples under a fixed normal load, N, ranging from 18.6 to 604.1 mN. The load was controlled using a mechanical balance to apply a constant dead weight. Samples were moved horizontally, relative to the indenter, using a variable speed motor (Newport ESP MFA-CC) at three velocities of $v=0.1$, 0.5, and 1 mm/s. Note that we controlled the normal load and not the vertical location of the indenter. For unstructured control samples in steady-state sliding, there is a corresponding steady-state film thickness profile. For the EMS samples, the film thickness profile changes periodically as the indenter traverses the spatially periodic structure. The indenter was connected to a load cell (Honeywell Precision Miniature Load Cell) measuring force in the direction of sample motion. Lubricated sliding experiments were conducted for at least one full cycle, where at the end of the cycle, the sample had returned to its starting

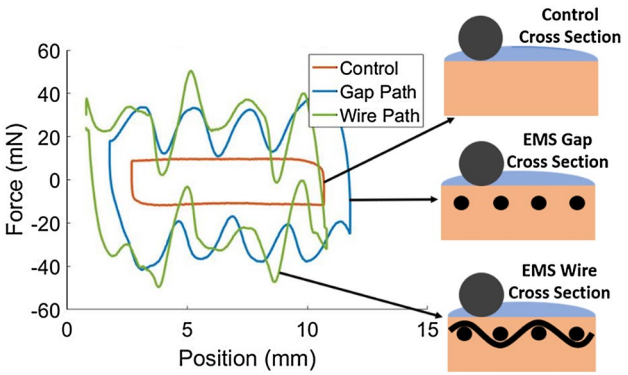

Fig. 2 Raw data from lubricated sliding experiments for a load of 238 mN, velocity of 0.1 mm/s, and a silicone oil lubricant with viscosity of 9.7 Pa*s. Data are shifted on the x-axis to match force peaks for illustration of difference in periodicity between two EMS paths

position. For the control, displacements per cycle were chosen such that the system had reached steady-state sliding (constant force value) over at least 1 mm of travel. For the EMS samples, displacement per cycle was kept at 10 mm so that multiple periods of the mesh structure were probed for each cycle. Two sliding paths were tested with the spherical indenter on the EMS samples. In the first, called the *gap path*, the center of the indenter slid through the center of the gap in the mesh, as detailed in the top schematic in Fig. 1d. In the second, called the *wire path*, the center of the indenter slid over the wire portion of the mesh at all times, as shown in the bottom schematic in Fig. 1d. Previous work using a silicone oil-based lubricant showed that swelling of the PDMS from the silicone oil was minimal and did not affect the mechanical properties of the system [14].

3 Results and Discussion

3.1 Experimental Analysis

Figure 2 shows typical data obtained from a lubricated sliding experiment for the control sample as well as the two indenter paths for the embedded mesh structure (EMS). The experiment was done under a normal load of 238 mN and a velocity of 0.1 mm/s, with a silicone oil lubricant of viscosity 9.7 Pa*s. The control exhibits steady-state sliding behavior, where the measured force is essentially constant in one direction of sliding. Conversely, the EMS sample shows large periodic fluctuations in sliding friction force for both the gap and wire paths. The experiment in which the indenter follows that the gap path shows a fluctuating force response with a period equal to that of the mesh. The experiment in which the indenter follows the wire path also shows a fluctuating response but with a period *twice* that of the mesh. It should be noted that for clarity, the curves for the two EMS paths are shifted to better visualize the periodic response by lining up the peak forces at the same location. We attribute this difference between the two paths to how the mesh is woven, which is illustrated by the schematics in Fig. 2. When sliding on the gap path, the wires over which the indenter travels are always at the same depth from the sample surface. However, when sliding on the wire path, the indenter travels over the section of the wires which is woven to form the mesh. Thus, for one mesh period the wire which the indenter slides on is woven over a perpendicular wire, and then the next mesh period the wire is woven under a perpendicular wire. This results in a repeated force response after about two periods of sliding for the wire path.

We obtain an average friction force, f, in terms of the energy lost in a cycle per unit distance traveled, which is computed as the integral of the data plotted in Fig. 2 such that

$$f = \oint P\mathrm{d}u/\delta, \tag{1}$$

where u is the displacement of the sample, P is the horizontal force measured experimentally, and δ is the distance traveled by the sample for a cycle. Using Eq. (1) to calculate friction force, it can be seen visually that the area of the curves in Fig. 2 for the EMS gap and wire path is significantly larger than the area of the control curve, meaning that the EMS samples have a larger friction force for the same conditions. It should be noted that the periodic nature of the EMS sample force curves also occurs under conditions where there is little to no enhancement (see SI, section S.2 for more details).

Figure 3a and b show plots of lubricated sliding friction coefficient, $\mu = f/N$, as a function of normal load, N, for velocities of 0.1 and 1 mm/s, respectively, with the lowest viscosity silicone oil as the lubricant ($\eta = 0.97$ Pa*s). For the velocity of 0.1 mm/s, Fig. 3a, the trend for the friction coefficient is similar for the two EMS paths but the magnitudes are larger for the wire path. For the control, at the lowest and highest loads, the friction coefficient is similar to the EMS samples. At intermediate loads, the control values are much smaller than the EMS values, meaning a substantial enhancement in sliding friction has occurred for both EMS paths. For the velocity of 1 mm/s, Fig. 3b, again the EMS sample shows friction enhancement, as for most loads tested, the control provides the smallest friction coefficient. When comparing samples across the two velocities, generally the sliding friction coefficient is larger for the lower velocity of 0.1 mm/s at the same loads.

It is useful to quantify the observed enhancement by calculating an enhancement ratio, ε, such that

$$\varepsilon = \frac{\mu_{\mathrm{EMS}}}{\mu_{\mathrm{Control}}}, \tag{2}$$

where μ_{EMS} and μ_{Control} are the experimental sliding friction coefficients for the EMS and control samples, respectively. Since there are two different indenter paths on the EMS sample, it is necessary to define two values of ε, $\varepsilon_{\mathrm{Gap}}$ and $\varepsilon_{\mathrm{Wire}}$. Enhancement ratios $\varepsilon_{\mathrm{Gap}}$ and $\varepsilon_{\mathrm{Wire}}$ are plotted in Fig. 3c and d, respectively, for the $\eta = 0.97$ Pa*s silicone oil lubricant and velocities of 0.1, 0.5, and 1 mm/s.

Figure 3c and d shows that for both indenter paths, the slowest velocity of 0.1 mm/s produced the largest sliding friction enhancements. The plot of $\varepsilon_{\mathrm{Gap}}$ vs load in Fig. 3c shows that, for all three velocities, friction enhancement is maximal at an intermediate value of load. At the lowest loads tested, there is little to no enhancement, and at high loads the enhancement ratio is likewise small. Peak enhancement ratios obtained at intermediate loads are 3.8, 2.4, and 1.8 for the velocities of 0.1, 0.5, and 1 mm/s, respectively. In the plot of $\varepsilon_{\mathrm{Wire}}$ vs load in Fig. 3d a similar trend is observed, except the peak enhancement ratio is larger with values of 5.8, 2.9, and 2.3 for velocities of 0.1, 0.5, and 1 mm/s, respectively. For both indenter paths, it appears that intermediate loads and low velocity conditions provide the optimal lubricated sliding friction enhancement.

To further investigate the experimental range in which the EMS structure is able to produce friction enhancements, two higher viscosity silicone oil lubricants ($\eta = 9.7$ Pa*s and 97 Pa*s) were used for the same velocity and load conditions as the 0.97 Pa*s viscosity silicone oil. As was the case for the lower viscosity silicone oil, the largest enhancements

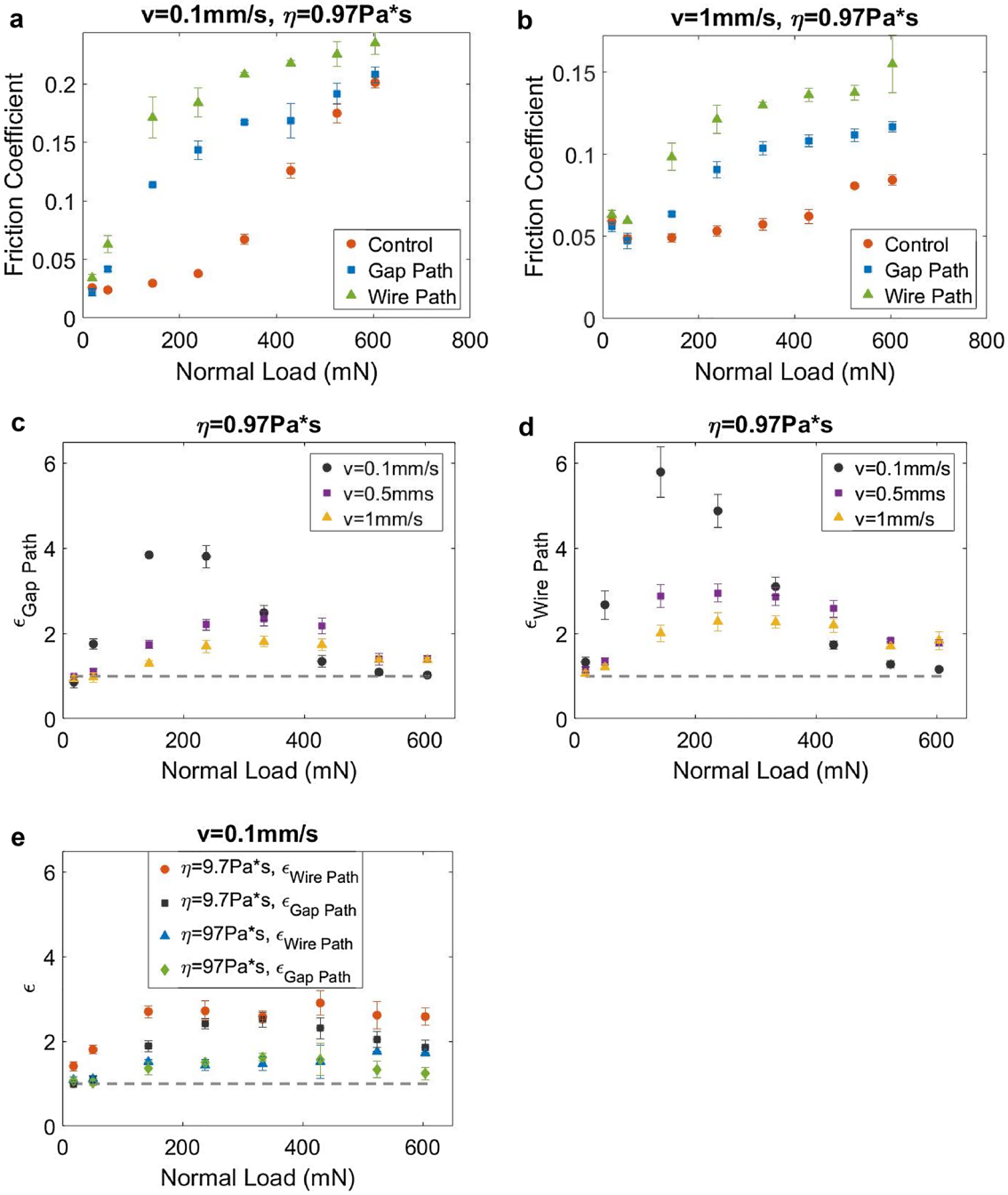

Fig. 3 **a**, **b** Lubricated friction coefficient vs normal load (18.62–604.1 mN) for the control and the EMS samples for 0.97 Pa*s viscosity silicone oil. **a** $v = 0.1$ mm/s, **b** $v = 1$ mm/s. **c**, **d** Enhancement ratio vs load for the EMS samples at $v = 0.1$, 0.5, and 1 mm/s for 0.97 Pa*s viscosity silicone oil. **c** Enhancement when sliding on the EMS gap path. **d** Enhancement when sliding on the EMS wire path. **e** Enhancement ratios for 9.7 and 97 Pa*s viscosity silicone oil at $v = 0.1$ mm/s. Gray-dashed line on enhancement ratio plots indicates value of 1 (no enhancement)

were obtained at the lowest experimental sliding velocity of 0.1 mm/s. Again, the wire path produced larger enhancements than the gap path for both silicone oils. Enhancement ratios for ε_{Gap} and ε_{Wire} at $v = 0.1$ mm/s are plotted for the two larger viscosity silicone oils in Fig. 3e. Enhancement ratio data for $v = 0.5$ and 1 mm/s can be found in the SI (S.2, Fig. S.2). For both ε_{Gap} and ε_{Wire}, it is observed that increasing the viscosity of the silicone oil to 9.7 Pa*s has resulted in a decrease in the peak magnitude of the enhancement with a maximum ε_{Gap} value of 2.5 and a maximum ε_{Wire} of 2.7. The peak enhancement is further lowered as the viscosity of the silicone oil is increased to 97 Pa*s with a maximum ε_{Gap}

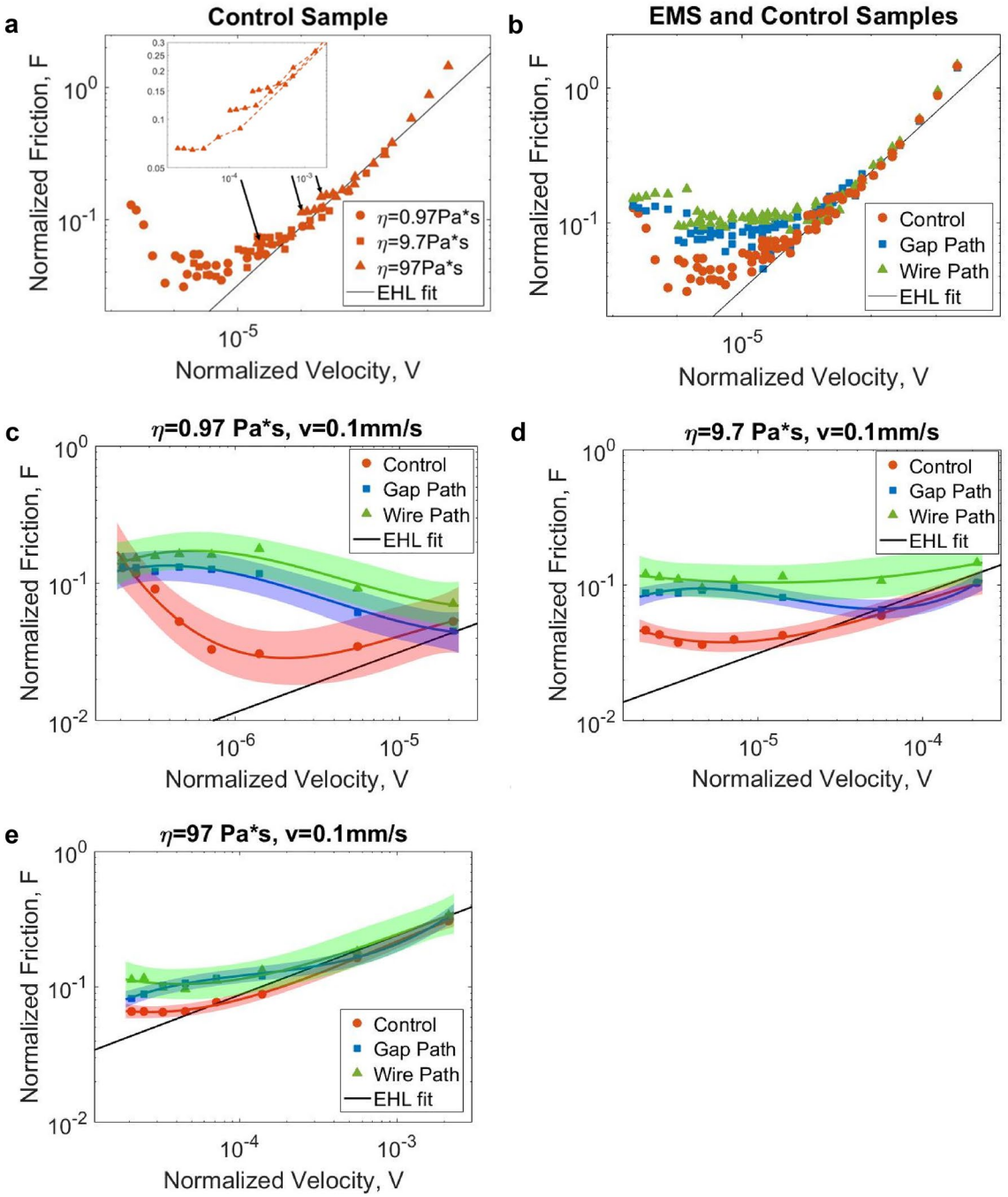

Fig. 4 **a**, **b** Plots of F vs V for **a** control samples, **b** control and EMS samples. **c**–**e** Plots of F vs V for the control, EMS gap path, and EMS wire path samples for a velocity of $v = 0.1$ mm/s. **c** 0.97 Pa*s, **d** 9.7 Pa*s, **e** 97 Pa*s. The shaded areas around the curves represent a 95% confidence interval for a third-order polynomial fit of the data. Black line in all plots is prediction from a modified version of the EHL model in Wu et al. [50] (Color figure online)

value of 1.6 and a maximum ε_{Wire} of 1.8. The overall trends of the data are similar for all three oils at low and intermediate loads, but at high loads, the enhancements observed for the higher viscosity silicone oils have not decreased to as small a value as it did for the lower viscosity silicone oil.

To better understand the enhancement mechanisms of the EMS sample, it is useful to investigate the lubrication regime of the system. Recent work using a two-phase periodic structure (TPPS) showed enhancements only when the system was in the EHL regime, caused by structure induced variations in the potential and elastic strain energies [14]. To investigate if a similar mechanism is driving the enhancements of the EMS samples, a scaling analysis was used to isolate which experimental conditions produced EHL behavior and which diverged from that behavior.

Isoviscous EHL theory shows that the friction response of a rigid sphere sliding on a lubricated homogeneous elastic substrate depends on a single dimensionless parameter V (normalized velocity) given by

$$V = \left(\eta R^{\frac{5}{3}} G^{\frac{1}{3}} N^{-\frac{4}{3}}\right) v, \tag{3}$$

where v is the sliding velocity, η is the lubricant viscosity, R is the indenter radius, G is the shear modulus of the elastic substrate, and N is the normal load [14, 49]. The corresponding normalized friction force, F, is such that

$$F = \left(R^{2/3} G^{1/3} N^{-4/3}\right) f = F(V). \tag{4}$$

That is, a signature of the EHL regime is that normalized friction, F is a function *only* of the normalized velocity V. We choose to display our experimental results using this EHL scaling. As shown below, data for different conditions collapse onto a single master curve within the EHL regime. Their divergence from a master curve, for example, under different velocities, then indicates departure of the system from the EHL regime.

Figure 4a shows EHL-scaled data for the control sample, plotting normalized friction, F, vs normalized velocity, V, for all experimental conditions tested. For all three viscosities, the portion of the data taken from low load experiments (high V) collapse onto a master curve. This master curve is fit with a previously published EHL model shown by the black line in Fig. 4a (details in SI, S.3) [50]. Model and experimental master curves are in good agreement at large values of V, suggesting that the system is in the EHL regime under those conditions. At higher loads (lower V), data diverge from the master curve and model. These divergences occur both for different viscosity lubricants and for different velocities tested using the same lubricant. For example, in the 97 Pa*s viscosity silicone oil experiments, shown as triangles in Fig. 4a, at low loads (high V), the data collapse onto the master curve for all three velocities tested ($v = 0.1$, 0.5, and 1 mm/s) suggesting EHL behavior. As load increases (V decreases), the data diverge from the master curve to form three separate curves where F decreases more slowly or remains constant with increasing load (decreasing V) (see inset plot in Fig. 4a). These three curves each represent one of the three velocities tested. This divergence from the master curve suggests that the higher load data are transitioning out of the EHL regime, meaning that experiments are probing multiple lubrication regimes. For the two lower viscosity silicone oil experiments (squares and circles), the low load experiments fall onto the same master curve as the higher viscosity silicone oil experiments (although there is more spread in the data). As the load increases (decreasing V), the same divergence into separate curves occurs. For the lowest viscosity silicone oil, as load is increased (V is decreased), F begins to increase steadily. An increase in force with a decrease in velocity is typically indicative of the mixed lubrication regime. Thus, analysis of the scaled control sample suggests that at low normal loads, the control is in the EHL regime, and as normal load is increased, the control transitions out of the EHL regime into the mixed lubrication regime.

Figure 4b shows the EHL-scaled data for the control sample and the wire and gap paths for the EMS sample for all experimental conditions tested. The EMS and control samples are scaled using the same value for shear modulus, G. In other words, the shear modulus for the PDMS matrix of the EMS samples is used, ignoring the embedded mesh. This is shown to be a good assumption at high values of V, where EMS data for both the wire and gap paths collapse onto the same master curve as the control samples, with good agreement to the EHL model. This indicates that at high values of V where samples exhibit EHL behavior, the embedded mesh structure has little effect on the mechanics of the lubricated contact and the samples behave as homogenous slabs of the matrix material. As V decreases, EMS sample data in Fig. 4b diverge from the EHL regime model *before* the control. This suggests that for the same experimental conditions, the control samples are in the EHL regime while the EMS samples are in or transitioning into the mixed lubrication regime. When this divergence occurs, the dimensionless friction is larger for the EMS samples than for the control samples at the same V, mirroring the friction enhancement of the EMS samples outlined previously in Fig. 3.

To further explore the effect of lubrication regime on the friction enhancement of EMS samples, the EHL normalized data for conditions which produced the largest friction enhancements of 3.8 and 5.8 for the gap and wire paths, respectively ($v = 0.1$ mm/s, $\eta = 0.97$ Pa*s silicone oil), are plotted in Fig. 4c along with the power-law (linear in a log–log plot) EHL model from Fig. 4a and b. Data in Fig. 4c are fit using a third-order polynomial, shown as the solid lines in the plots. Also shown is a 95% confidence interval

represented by the shaded area around each curve (details in the SI, S.4). Looking at the lubrication regime behavior of the sample in Fig. 4c can give insight to the mechanisms for the friction enhancement ratios obtained for these conditions discussed previously for Fig. 3c and d. In Fig. 3c and d, enhancement ratios for both paths at $v = 0.1$ mm/s start off with little to no enhancement at low loads, which corresponds to large V in Fig. 4c, where the three curves overlap. As load increases in Fig. 3c and d, enhancement ratio increases. This corresponds to decreasing V in Fig. 4c, where at first for the control sample, we see typical EHL behavior (decreasing F with decreasing V), but for the EMS samples, we see only non-EHL behavior (increasing F with decreasing V). This suggests that at these conditions, the EMS samples are operating in the mixed lubrication regime while the control is operating in the EHL regime. This difference between the EMS and control samples creates a divergence in the lubricated friction response, with larger frictional forces occurring for the EMS samples. It results in the friction enhancements seen in Fig. 3c and d at intermediate loads. Thus, it appears that the cause of the observed enhancements in friction is that with increasing load, the EMS samples leave the EHL regime and enter the mixed lubrication regime before the control sample. This hypothesis is supported by behavior at low V, where the control sample in Fig. 4c begins to show a non-EHL regime response (increasing F with decreasing V) and the curves for the EMS and control samples converge. This corresponds to large loads in Fig. 3c and d, where the enhancement is lost. With increasing load, the control sample also enters the mixed lubrication regime, leading eventually to a loss of friction enhancement for the EMS samples.

Figure 4d and e shows F versus V for the same velocity presented in Fig. 4c ($v = 0.1$ mm/s) and larger viscosity silicone oils ($\eta = 9.7$ and 97 Pa*s, respectively). Again, conditions where the EMS samples and control are in different lubrication regimes correspond to conditions in which friction enhancements are observed in the EMS samples, shown in Fig. 3e. Figure 4d corresponds to conditions which produced enhancement ratios of up to 2.5 and 2.7 for the EMS gap and wire paths, respectively. These enhancement values are lower than those seen for the data in Fig. 4c. Transition to EHL-like behavior is observed for the EMS sample in Fig. 4d at large values of V, especially for the gap path. As V decreases, the EMS samples again diverge from the EHL scaling behavior before the control does, leading to friction enhancements. Figure 4e shows conditions which produced friction enhancements peaking at 1.6 and 1.8 for the EMS gap and wire path, respectively. All three samples follow the EHL model very well at large values of V, with divergence occurring more modestly than in Fig. 4c and d at intermediate and small values of V. Figure 4c–e shows that the friction enhancements obtained for the EMS samples with increasing load appear to be dependent on both the divergence from EHL regime before the control sample as well as that divergence being significant in magnitude.

Figure 4c–e shows that viscosity of the silicone oil has a strong effect on the lubrication regime behavior between the samples. The lowest viscosity silicone oil showed the largest magnitude enhancement ratios between the EMS and control samples and showed no EHL behavior at high values of V for either of the EMS samples. As the viscosity of the silicone oil was increased, the peak enhancement ratios decreased and the EMS samples began to exhibit more EHL-like behavior at the largest values of V. The larger viscosity silicone oils producing EHL regime behavior for the EMS samples likely have to do with the lubricant film thickness increasing with an increase in viscosity under the same load and velocity conditions. This can shift the samples from the mixed regime into the EHL regime. It is not clear though, why the larger viscosity silicone oils produce more similar transitions out of the EHL regime between the EMS and control samples, resulting in lower enhancement ratios.

The observation of significant friction enhancements when conditions are outside of the EHL regime is in stark contrast to those for the previously developed TPPS, which only exhibited lubricated sliding friction enhancements while in the EHL regime [14]. The TPPS structure relied on energy losses through the lubricant as potential and elastic strain energies of the system varied periodically with sliding over different phases of the sample. Once the system entered the mixed lubrication regime, the sliding friction instead became dominated by forces with larger magnitudes, such as adhesive and viscoelastic forces. These forces produced similar friction responses for the TPPS and control sample, and thus, enhancement was lost. Since the EMS sample enters the mixed lubrication regime before the control sample when enhancements are observed, these forces produce a larger friction response for the EMS samples. Once the control also enters the mixed lubrication regime, the forces acting on both samples become more similar and sometimes equivalent, eliminating enhancements, similar to what was observed for the TPPS samples. The force response of the samples (both control and EMS) individually follows what is expected for transitions between EHL and mixed lubrication regime behavior. The novel question for the system is the mechanism for the early departure from EHL regime behavior for the EMS samples when compared to the control samples, which likely occurs as a response to the mesh structure.

We consider two ways to interpret the friction data. In the first, which we adopt as argued below, variation in force is ascribed to be due to smooth sliding of the indenter over a material with spatial variation of contact stiffness. In the second interpretation, periodic variation of the friction, Fig. 2, is due to stick–slip events.

The EMS samples show periodic variation of friction even in the EHL regime when there solid surfaces are separated by a full fluid film (thus there is no dry contact). This argues against the stick–slip interpretation (see also SI, Fig. S.1). Moreover, the signature of stick–slip during friction is alternation between (a) arrested displacement (during which force builds up linearly) and (b) dynamic instability (during which the force falls precipitously). This typically results in a "sawtooth" force pattern. The force trace for the EMS sample data, especially for the gap path, is stable and smooth. This is consistent with the first interpretation: that the periodicity is a result of smooth sliding on a surface with periodic variation of properties (in this case local modulus [14]). Finally, we find that there is no periodicity of the friction force in the control samples, consistent with the first interpretation. For the second interpretation, in contrast, we would expect stick–slip to occur even for the control samples. Moreover, even when the control sample is in the mixed lubrication regime, there is no sign of stick–slip behavior. For these reasons, we adopt the first interpretation that periodicity of friction force is due to smooth sliding on a substrate with periodic variation of contact stiffness.

The EHL scaling analysis shows that the EMS samples behave as homogeneous slabs of the matrix material in the EHL regime (see Fig. 4b). As V decreases, some phenomenon occurs which causes them to diverge from the EHL regime before the control samples. The effect of the mesh on the effective homogeneous composite modulus of the EMS samples is unlikely to cause this divergence. Stiffer elastomers have been studied in previous work, and additional higher modulus silicone elastomer data can be found in the SI (S.5, Fig. S.2). Results for these stiffer elastomers show that materials with uniformly higher modulus result in decreased lubricated friction compared to the lower modulus control sample under the experimental conditions covered in this work [14]. Rather, it is possible the local, spatially varying, contact stiffness of the EMS sample is contributing to the lubricated sliding behavior. It has been suggested that for a particle/rubber composite the local hardness of the contact can play a role [7, 8]. Experiments have shown that harder particles can result in breaking of lubricant films more easily than softer particles. This allows for additional solid–solid contact to occur during lubricated sliding, resulting in a larger friction. This mechanism could be occurring with the EMS structure, where when the indenter is sliding over the wires of the mesh, it is probing a finite area of much larger local contact stiffness than that of the soft elastomer matrix, resulting in a larger local pressure. Larger

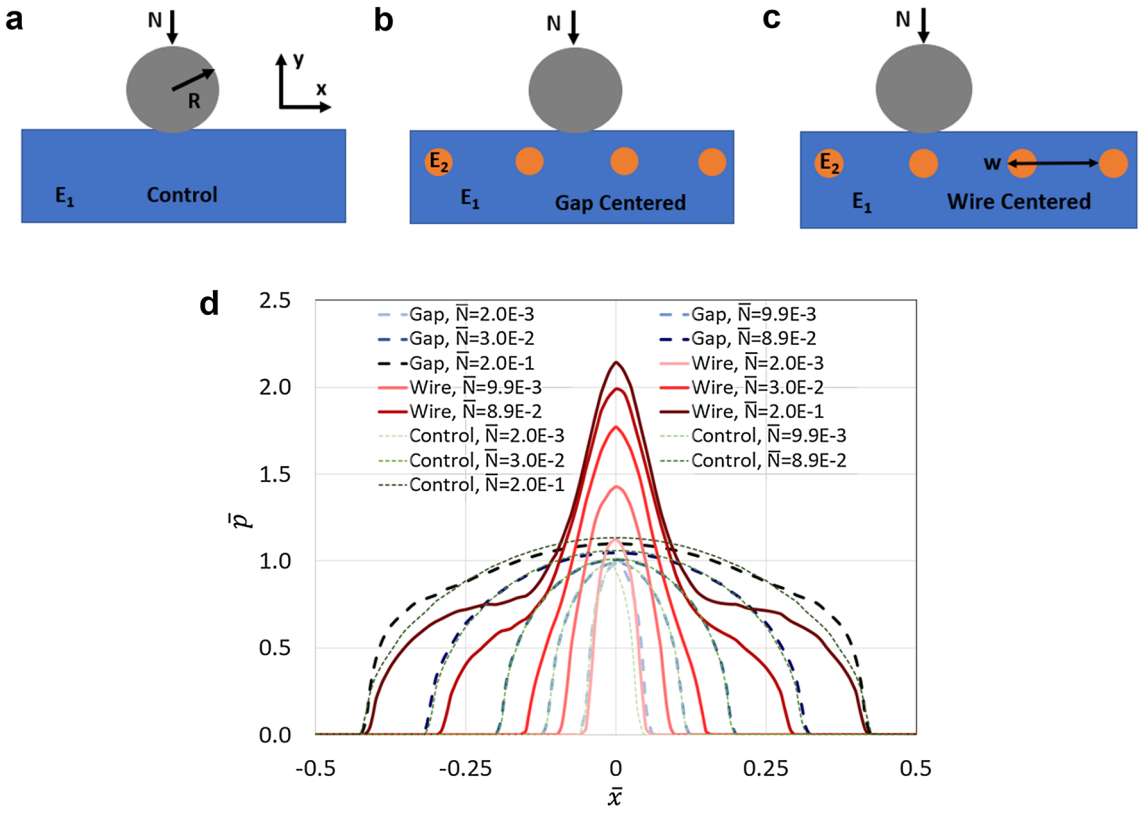

Fig. 5 **a**–**c** Schematic of sections investigated using FEM. **a** Schematic of control simulation, **b** schematic of gap-centered simulation, **c** schematic of wire-centered simulation. **d** Plot of $\bar{p}$ vs $\bar{x}$ from FEM simulations.

local pressure, we hypothesize, promotes earlier breakage of the lubricant film than for the control sample. This could explain the shift of the EMS samples towards the mixed lubrication regime under conditions where the control is still in the EHL regime. This could also explain the differences in enhancement ratio magnitudes observed for the different viscosity silicone oils. All silicone oils appear to have reached peak enhancement ratios under the conditions tested, but the smallest viscosity silicone oil produced substantially larger enhancement ratios. If the lower viscosity silicone oil lubricant film was less stable, it could result in more film breakage and have more solid–solid contact adding to the friction response.

3.2 Finite Element Analysis

To investigate the hypothesis that differences in local pressures are related to differences in the conditions for transition to the mixed lubrication regime, a finite element model was developed (details in SI, S.7). The model simulates indentation of a flat sample with a circular indenter in a 2D analog of the experimental geometry. Simulations have no fluid present and instead the surfaces are treated as frictionless. This simplification is applied due to the compliance of the samples. Previous work showed that under sufficiently compliant conditions, the film thickness in the contact region is very small compared to the contact width and depth, and contact pressure is accurately approximated by the corresponding dry Hertz problem [50]. Schematics with the geometry of the simulations are shown in Fig. 5a–c. All simulations have samples indented under a fixed normal load N. For the control sample in Fig. 5a, the indenter is in contact with a sample of homogeneous elastic material of modulus E_1. For the gap-centered and wire-centered samples in Fig. 5b and c, the sample comprises a matrix of elastic material with modulus E_1 which contains circular segments of a stiffer material of modulus E_2 embedded below the surface of the sample. For the gap-centered simulation in Fig. 5b, the center of the indenter is positioned between two stiff circular segments, to model when the experimental indenter is in the middle of the gap of the wire mesh, which occurs during portions of the gap path experiments. For the wire-centered simulation in Fig. 5c, the center of the indenter is positioned over the center of one of the rigid circular segments, to model when the experimental indenter is traveling over the wire, which occurs at some times during the gap experiments and at all times during the wire path experiments.

The Hertz contact pressure for a rigid cylinder in contact with a homogeneous elastic half space is

$$p_H = p_{\max}\sqrt{1-\frac{x^2}{a^2}}, \tag{5}$$

$$p_{\max} = \frac{2N}{\pi a}, \tag{6}$$

where a is the contact half-width and x is the location on the contacting surfaces [51]. In terms of the applied load N, a is given by

$$a^2 = \frac{4NR}{\pi E^*}, \tag{7}$$

$$\frac{1}{E^*} = \frac{1-\nu^2}{E}, \tag{8}$$

$$p_H = \frac{2N}{\pi a}\sqrt{1-\frac{\pi E^* x^2}{4NR}}, \tag{9}$$

where E is the Young's modulus of the PDMS, R is the radius of the indenter, and ν is the Poisson ratio. Here, we use this solution to normalize pressure in our experiments. Specifically, we normalize pressure by $p_{\max}$ given by Eqs. (6) and (7):

$$\overline{p} = \frac{p}{p_{\max}} \tag{10}$$

and

$$\overline{x} = \frac{x}{w}; \overline{R} = \frac{R}{w}; \overline{N} = \frac{N}{wE^*} \tag{11}$$

where w is the period of the embedded structure.

Plots of normalized pressure $\overline{p}$ vs $\overline{x}$ for five different values of $\overline{N}$ are shown in Fig. 5d. The origin indicates the center point of contact with the indenter. The pressure profiles for the control- and gap-centered simulation are similar for all values of $\overline{N}$, though at the largest value, the curves diverge far from the contact center. The maximum value of $\overline{p}$ for the control is close to one for all values of $\overline{N}$. It is not exactly one because of the finite thickness of the sample ($p_{\max}$ in Eq. (6) is for an elastic half space). For the wire-centered simulation, at the smallest value of N, the shape of the curve is similar to the control- and gap-centered simulations, but the maximum $\overline{p}$ is larger. As $\overline{N}$ increases in the wire-centered simulations, the maximum $\overline{p}$ becomes significantly larger than the control and the shape of the pressure profile changes into one with two distinct regions. Specifically, near the center of the contact region, we find a sharp increase in pressure.

These simulations show that the pressure profile of the embedded structure is very dependent on indenter location. When the indenter is centered over the gap between embedded structures, the pressure profile is similar to that of the control. When the indenter is centered over the embedded structure, much larger pressures are obtained locally at the center of contact. For a lubricated sample, this sharp

increase in local pressure would likely result in a thinner fluid film. This thin film will be less stable and more likely to break allowing for solid–solid contact, which can cause large increases in the lubricated friction response and deviation from EHL behavior. This supports observations that the EMS samples enter the mixed regime at lower loads than the control sample. It also gives insight to why the largest enhancements are observed for the wire path rather than the gap path. For the wire path, the indenter is in a configuration similar to the wire-centered simulation in Fig. 5c at all times, where we obtain substantially larger pressures for all loads when compared to the control sample. For the gap path experiments, the indenter fluctuates between the wire-centered simulation in Fig. 5c and the gap-centered simulation in Fig. 5b where the pressure is similar to the control. This suggests that the gap path experiments behave as a mixture of control behavior and wire path behavior, resulting in friction forces that fall between the two. Thus, it appears that the friction enhancements observed for the EMS samples could be a product of local areas of high pressure between the contacting surfaces, induced by the local stiffness of the structure in the sample.

4 Conclusions

A structure comprising a plastic mesh embedded in a compliant elastomer matrix was developed. This embedded mesh structure (EMS) was found to have increased lubricated sliding friction when compared to a control sample of just the compliant elastomer material. Analysis suggests that enhancements occur when the EMS sample is operating in the mixed lubrication regime under conditions where the control is in the EHL regime or is just beginning to transition out of the EHL regime. It is proposed that the early transition of the EMS sample into the mixed lubrication regime is caused by structure induced pressure spikes causing thinning and destabilization of the fluid film. Indentation simulations supporting this mechanism showed increased pressure at the center of contact when the indenter was centered over an embedded structure, and control-like pressure profiles when the indenter was centered away from an embedded structure. Thus, the local stiffness of a surface may play a role in the lubrication behavior of nonhomogeneous contacts.

Supplementary Information The online version contains supplementary material available at https://doi.org/10.1007/s11249-021-01540-9.

Acknowledgements We thank Prof. Kelly Schultz for use of the rheometer to measure PDMS Young's modulus.

Funding We acknowledge support from the National Science Foundation through the Grant LEAP-HI: CMMI-1854572.

Declarations

Conflict of interest The authors have no financial or non-financial interests to disclose.

References

1. Manning, D.P., Jones, C., Rowland, F.J., Roff, M.: The surface roughness of a rubber soling material determines the coefficient of friction on water-lubricated surfaces. J. Saf. Res. **29**(4), 275–283 (1998)
2. Li, K.W., Chen, C.J.: The effect of shoe soling tread groove width on the coefficient of friction with different sole materials, floors, and contaminants. Appl. Ergon. **35**(6), 499–507 (2004)
3. Harrin, E.: Low tire friction and cornering forces on a wet surface. Wear **2**(6), 492 (1959)
4. Sabey, B.E., Lupton, G.N.: Friction on wet surfaces of tire-tread-type vulcanizates. Rubber Chem. Technol. **37**(4), 878–893 (1964)
5. Grosch, K.A., Schallamach, A.: Tire friction on wet roads. Rubber Chem. Technol. **49**(3), 862–908 (1976)
6. Klüppel, M., Bomal, Y., Le Gal, A., Guy, L., Orange, G.: Modelling of sliding friction for carbon black and silica filled elastomers on road tracks. Wear **264**(7–8), 606–615 (2007)
7. Wang, Y.X., Ma, J.H., Zhang, L.Q., Wu, Y.P.: Revisiting the correlations between wet skid resistance and viscoelasticity of rubber composites via comparing carbon black and silica fillers. Polym. Test. **30**(5), 557–562 (2011)
8. Wang, Y.X., Wu, Y.P., Li, W.J., Zhang, L.Q.: Influence of filler type on wet skid resistance of SSBR/BR composites: effects from roughness and micro-hardness of rubber surface. Appl. Surf. Sci. **257**(6), 2058–2065 (2011)
9. Muller, H.K.: Fluid Sealing Technology: Principles and Applications. Routledge, London (1998)
10. Jin, Z.M., Dowson, D.: Elastohydrodynamic lubrication in biological systems. Proc. Inst. Mech. Eng. J **219**(5), 367–380 (2005)
11. Sawyer, W.G., Dunn, A.C., Tichy, J.A., Uruen, J.M.: Lubrication regimes in contact lens wear during a blink. Tribol. Int. **63**, 45–50 (2013)
12. Adams, M.J., Briscoe, B.J., Johnson, S.A.: Friction and lubrication of human skin. Tribol. Lett. **26**(3), 239–253 (2007)
13. Malone, M.E., Appelqvist, I.A.M., Norton, I.T.: Oral behaviour of food hydrocolloids and emulsions. Part 1. Lubrication and deposition considerations. Food Hydrocoll. **17**(6), 763–773 (2003)
14. Moyle, N., Wu, H., Khripin, C., Bremond, F., Hui, C.-Y., Jagota, A.: Enhancement of elastohydrodynamic friction by elastic hysteresis in a periodic structure. Soft Matter **16**, 1627–1635 (2020)
15. Cameron, A.: Basic Lubrication Theory. E. Horwood, Chichester (1976)
16. Dowson, D., Higginson, G.R., Archard, J.F., Crook, A.W.: Elasto-Hydrodynamic Lubrication. Pergamon Press, Oxford (1977)
17. Persson, B.N.J.: Sliding Friction, Physical Principles and Applications. Springer-Verlag, Berlin (2000)
18. Martz, B.L.S.: Preliminary report of developments in interrupted surface finishes. Proc. Inst. Mech. Eng. **16**(1), 1–9 (1947)
19. Okrent, E.H.: The effect of lubricant viscosity and composition on engine friction and bearing wear. ASLE Trans. **4**(1), 97–108 (1961)
20. Tzeng, S.T., Saibel, E.: Surface roughness effect on slider bearing lubrication. ASLE Trans. **10**(3), 334–348 (1967)
21. McGeehan, J.A.: A literature review of the effects of piston and ring friction and lubricating oil viscosity on fuel economy. SAE Trans. **87**, 2619–2638 (1978)

22. Persson, B.N.J., Scaraggi, M.: On the transition from boundary lubrication to hydrodynamic lubrication in soft contacts. J. Phys. Condens. Matter **21**(18), 185002 (2009)
23. Skotheim, J.M., Mahadevan, L.: Soft lubrication. Phys. Rev. Lett. (2004). https://doi.org/10.1103/PhysRevLett.92.245509
24. Skotheim, J.M., Mahadevan, L.: Soft lubrication: the elastohydrodynamics of nonconforming and conforming contacts. Phys. Fluids **17**(9), 1–23 (2005)
25. Scaraggi, M., Carbone, G., Persson, B.N.J., Dini, D.: Lubrication in soft rough contacts: a novel homogenized approach. Part I—theory. Soft Matter **7**(21), 10395–10406 (2011)
26. Pandey, A., Karpitschka, S., Venner, C.H., Snoeijer, J.H.: Lubrication of soft viscoelastic solids. J. Fluid Mech. **799**, 433–447 (2016)
27. De Vicente, J., Stokes, J.R., Spikes, H.A.: The frictional properties of Newtonian fluids in rolling—sliding soft-EHL contact. Tribol. Lett. **20**(3–4), 273–286 (2005)
28. Bongaerts, J.H.H., Fourtouni, K., Stokes, J.R.: Soft-tribology: lubrication in a compliant PDMS-PDMS contact. Tribol. Int. **40**(10–12), 1531–1542 (2007)
29. Scaraggi, M., Carbone, G., Dini, D.: Experimental evidence of micro-EHL lubrication in rough soft contacts. Tribol. Lett. **43**(2), 169–174 (2011)
30. Kim, J.M., Wolf, F., Baier, S.K.: Effect of varying mixing ratio of PDMS on the consistency of the soft-contact Stribeck curve for glycerol solutions. Tribol. Int. **89**, 46–53 (2015)
31. Stupkiewicz, S., Lengiewicz, J., Sadowski, P., Kucharski, S.: Finite deformation effects in soft elastohydrodynamic lubrication problems. Tribol. Int. **93**, 511–522 (2016)
32. Selway, N., Chan, V., Stokes, J.R.: Influence of fluid viscosity and wetting on multiscale viscoelastic lubrication in soft tribological contacts. Soft Matter **13**(8), 1702–1715 (2017)
33. Sadowski, P., Stupkiewicz, S.: Friction in lubricated soft-on-hard, hard-on-soft and soft-on-soft sliding contacts. Tribol. Int. **129**, 246–256 (2019)
34. Tan, G., Wang, D., Liu, S., Wang, H., Zhang, S.: Frictional behaviors of rough soft contact on wet and dry pipeline surfaces: with application to deepwater pipelaying. Sci. China Technol. Sci. **56**(12), 3024–3032 (2013)
35. Deleau, F., Mazuyer, D., Koenen, A.: Sliding friction at elastomer/glass contact: influence of the wetting conditions and instability analysis. Tribol. Int. **42**(1), 149–159 (2009)
36. Pan, X.D.: Wet sliding friction of elastomer compounds on a rough surface under varied lubrication conditions. Wear **262**(5–6), 707–717 (2007)
37. Pan, X.: Contribution of fine filler particles to energy dissipation during wet sliding of elastomer compounds on a rough surface. J. Phys. D **40**(15), 4657–4667 (2007)
38. Gropper, D., Wang, L., Harvey, T.J.: hydrodynamic lubrication of textured surfaces: a review of modeling techniques and key findings. Tribol. Int. **94**, 509–529 (2016)
39. Varenberg, M., Gorb, S.N.: Hexagonal surface micropattern for dry and wet friction. Adv. Mater. **21**(4), 483–486 (2009)
40. Peng, Y., Serfass, C.M., Hill, C.N., Hsiao, L.C.: Bending of soft micropatterns in elastohydrodynamic lubrication tribology. Exp. Mech. **61**(6), 969–979 (2021)
41. Peng, Y., Serfass, C.M., Kawazoe, A., Shao, Y., Gutierrez, K., Hill, C.N., Santos, V.J., Visell, Y., Hsiao, L.C.: Elastohydrodynamic friction of robotic and human fingers on soft micropatterned substrates. Nat. Mater. (2021). https://doi.org/10.1038/s41563-021-00990-9
42. Moyle, N., He, Z., Wu, H., Hui, C.Y., Jagota, A.: Indentation versus rolling: dependence of adhesion on contact geometry for biomimetic structures. Langmuir **34**(13), 3827–3837 (2018)
43. He, Z., Moyle, N.M., Hui, C.Y., Levrard, B., Jagota, A.: Adhesion and friction enhancement of film-terminated structures against rough surfaces. Tribol. Lett. **65**(4), 161 (2017)
44. Mengüç, Y., Sitti, M.: Gecko-inspired polymer adhesives. Polym. Adhes. Frict. Lubr. (2013). https://doi.org/10.1002/9781118505175.ch9
45. Murphy, M.P., Aksak, B., Sitti, M.: Adhesion and anisotropic friction enhancements of angled heterogeneous micro-fiber arrays with spherical and spatula tips. J. Adhes. Sci. Technol. **21**(12), 1281–1296 (2007)
46. Reddy, S., Arzt, E., del Campo, A., Del Campo, A.: Bioinspired surfaces with switchable adhesion. Adv. Mater. **19**(22), 3833–3837 (2007)
47. Liu, J., Hui, C.-Y., Jagota, A.: Effect of fibril arrangement on crack trapping in a film-terminated fibrillar interface. J. Polym. Sci. B **47**(23), 2368–2384 (2009)
48. Jagota, A., Hui, C.Y.: Adhesion, friction, and compliance of bio-mimetic and bio-inspired structured interfaces. Mater. Sci. Eng. R **72**(12), 253–292 (2011)
49. Snoeijer, J.H., Eggers, J., Venner, C.H.: Similarity theory of lubricated Hertzian contacts. Phys. Fluids (2013). https://doi.org/10.1063/1.4826981
50. Wu, H., Moyle, N., Jagota, A., Hui, C.-Y.: Lubricated steady sliding of a rigid sphere on a soft elastic substrate: hydrodynamic friction in the Hertz limit. Soft Matter **16**, 2760–2773 (2020)
51. Johnson, K.L.: Contact Mechanics. Cambridge University Press, Cambridge (1985)